

SHORT COMMUNICATION

Androgenetic/biparental mosaicism in a girl with Beckwith–Wiedemann syndrome-like and upd(14)pat-like phenotypes

Kazuki Yamazawa^{1,5}, Kazuhiko Nakabayashi², Kentaro Matsuoka³, Keiko Masubara¹, Kenichiro Hata², Reiko Horikawa⁴ and Tsutomu Ogata¹

This report describes androgenetic/biparental mosaicism in a 4-year-old Japanese girl with Beckwith–Wiedemann syndrome (BWS)-like and paternal uniparental disomy 14 (upd(14)pat)-like phenotypes. We performed methylation analysis for 18 differentially methylated regions on various chromosomes, genome-wide microsatellite analysis for a total of 90 loci and expression analysis of *SNRPN* in leukocytes. Consequently, she was found to have an androgenetic 46,XX cell lineage and a normal 46,XX cell lineage, with the frequency of the androgenetic cells being roughly calculated as 91% in leukocytes, 70% in tongue tissues and 79% in tonsil tissues. It is likely that, after a normal fertilization between an ovum and a sperm, the paternally derived pronucleus alone, but not the maternally derived pronucleus, underwent a mitotic division, resulting both in the generation of the androgenetic cell lineage by endoreplication of one blastomere containing a paternally derived pronucleus and in the formation of the normal cell lineage by union of paternally and maternally derived pronuclei. It appears that the extent of overall (epi)genetic aberrations exceeded the threshold level for the development of BWS-like and upd(14)pat-like phenotypes, but not for the occurrence of other imprinting disorders or recessive Mendelian disorders.

Journal of Human Genetics (2011) 56, 91–93; doi:10.1038/jhg.2010.142; published online 11 November 2010

Keywords: androgenesis; Beckwith–Wiedemann syndrome; mosaicism; upd(14)pat

INTRODUCTION

A pure androgenetic human with paternal uniparental disomy for all chromosomes is incompatible with life because of genomic imprinting.^{1,2} However, a human with an androgenetic cell lineage could be viable in the presence of a normal cell lineage. Indeed, an androgenetic cell lineage has been identified in six liveborn individuals with variable phenotypes.^{3–7} All the androgenetic cell lineages have a 46,XX karyotype, and this is consistent with the lethality of an androgenetic 46,YY cell lineage.

Here, we report on a girl with androgenetic/biparental mosaicism, and discuss the underlying factors for the phenotypic development.

CASE REPORT

This patient was conceived naturally to non-consanguineous and healthy parents. At 24 weeks gestation, the mother was referred to us because of threatened premature delivery. Ultrasound studies showed Beckwith–Wiedemann syndrome (BWS)-like features,⁸ such as macroglossia, organomegaly and umbilical hernia, together with

polyhydramnios and placentomegaly. The mother repeatedly received amnioreduction and tocolysis.

She was delivered by an emergency cesarean section because of preterm rupture of membranes at 34 weeks of gestation. Her birth weight was 3730 g (+4.8 s.d. for gestational age), and her length 45.6 cm (+0.7 s.d.). The placenta weighed 1040 g (+7.3 s.d.).⁹ She was admitted to a neonatal intensive care unit due to asphyxia. Physical examination confirmed a BWS-like phenotype. Notably, chest roentgenograms delineated mild bell-shaped thorax characteristic of paternal uniparental disomy 14 (upd(14)pat),¹⁰ although coat hanger appearance of the ribs indicative of upd(14)pat was absent (Supplementary Figure 1). She was placed on mechanical ventilation for 2 months, and received tracheostomy, glossectomy and tonsillectomy in her infancy, due to upper airway obstruction. She also had several clinical features occasionally reported in BWS⁸ (Supplementary Table 1). Her karyotype was 46,XX in all the 50 lymphocytes analyzed. On the last examination at 4 years of age, she showed postnatal growth failure and severe developmental retardation.

¹Department of Molecular Endocrinology, National Research Institute for Child Health and Development, Tokyo, Japan; ²Department of Maternal-Fetal Biology, National Research Institute for Child Health and Development, Tokyo, Japan; ³Division of Pathology, National Medical Center for Children and Mothers, Tokyo, Japan and ⁴Division of Endocrinology and Metabolism, National Medical Center for Children and Mothers, Tokyo, Japan

⁵Current address: Department of Physiology, Development & Neuroscience, University of Cambridge, Cambridge, UK.

Correspondence: Dr T Ogata, Department of Molecular Endocrinology, National Research Institute for Child Health and Development, 2-10-1 Ohkura, Setagaya, Tokyo 157-8535, Japan.

E-mail: tomogata@nch.go.jp

Received 9 September 2010; revised 18 October 2010; accepted 22 October 2010; published online 11 November 2010

MOLECULAR STUDIES

This study was approved by the Institutional Review Board Committee at the National Center for Child health and Development, and performed after obtaining informed consent.

Methylation analysis

We first performed bisulfite sequencing for the *H19*-DMR (differentially methylated region) and *KvDMR1* as a screening of BWS^{11,12} and that for the *IG*-DMR and the *MEG3*-DMR as a screening of upd(14)pat,¹⁰ using leukocyte genomic DNA. Paternally derived clones were predominantly identified for the four DMRs examined (Figure 1a). We next performed combined bisulfite restriction analysis for multiple DMRs, as reported previously.¹³ All the autosomal DMRs exhibited markedly skewed methylation patterns consistent with predominance of paternally inherited clones, whereas the *XIST*-DMR on the X chromosome showed a normal methylation pattern (Figure 1a).

Genome-wide microsatellite analysis

Microsatellite analysis was performed for 90 loci with high heterozygosities in the Japanese population.¹⁴ Major peaks consistent with paternal uniparental isodisomy and minor peaks of maternal origin were identified for at least one locus on each chromosome, with the minor peaks of maternal origin being more obvious in tongue and

tonsil tissues than in leukocytes (Figure 1b and Supplementary Table 2). There were no loci with three or four peaks indicative of chimerism. The frequency of the androgenetic cells was calculated as 91% in leukocytes, 70% in tongue cells and 79% in tonsil cells, although the estimation apparently was a rough one (for details, see Supplementary Methods).

Expression analysis

We examined *SNRPN* expression, because *SNRPN* showed strong expression in leukocytes (for details, see Supplementary Data). *SNRPN* expression was almost doubled in the leukocytes of this patient (Figure 1c).

DISCUSSION

These results suggest that this patient had an androgenetic 46,XX cell lineage and a normal 46,XX cell lineage. In this regard, both the androgenetic and the biparental cell lineages appear to have derived from a single sperm and a single ovum, because a single haploid genome of paternal origin and that of maternal origin were identified in this patient by genome-wide microsatellite analysis. Thus, it is likely that after a normal fertilization between an ovum and a sperm, the paternally derived pronucleus alone, but not the maternally derived pronucleus, underwent a mitotic division, resulting both in the generation of the androgenetic cell lineage by endoreplication of

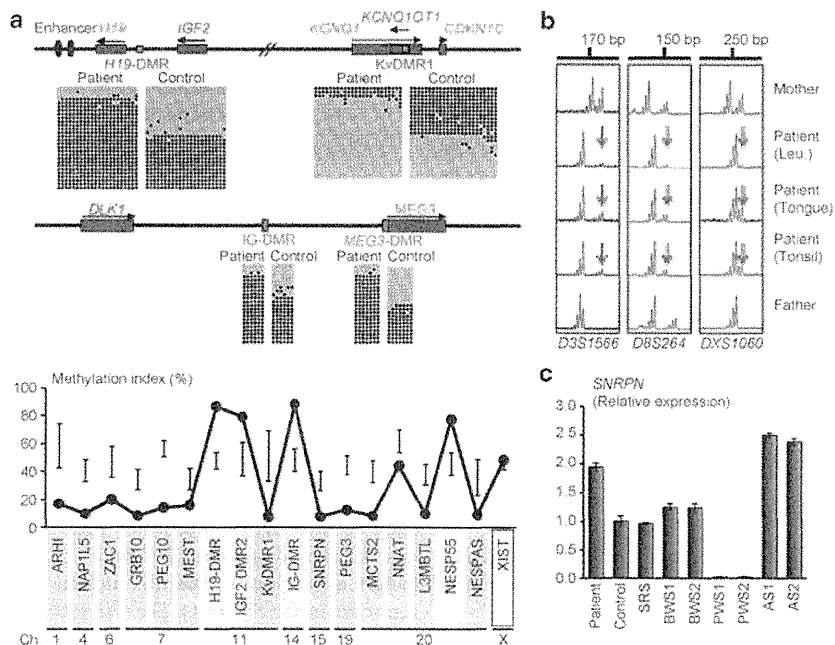


Figure 1 Representative molecular results. (a) Methylation analysis. Upper part: Bisulfite sequencing data for the *H19*-DMR and the *KvDMR1* on 11p15.5, and those for the *IG*-DMR and the *MEG3*-DMR on 14q32.2. Each line indicates a single clone, and each circle denotes a CpG dinucleotide; filled and open circles represent methylated and unmethylated cytosines, respectively. Paternally expressed genes are shown in blue, maternally expressed gene in red, and the DMRs in green. The *H19*-DMR, the *IG*-DMR, and the *MEG3*-DMR are usually methylated after paternal transmission and unmethylated after maternal transmission, whereas the *KvDMR1* is usually unmethylated after paternal transmission and methylated after maternal transmission.^{10,11} Lower part: Methylation indices (the ratios of methylated clones) obtained from the COBRA analyses for the 18 DMRs. The DMRs highlighted in blue and pink are methylated after paternal and maternal transmissions, respectively. The black vertical bars indicate the reference data (maximum – minimum) in leukocyte genomic DNA of 20 normal control subjects (the *XIST*-DMR data are obtained from 16 control females). (b) Representative microsatellite analysis. Major peaks of paternal origin and minor peaks of maternal origin (red arrows) have been identified in this patient. The minor peaks of maternal origin are more obvious in tongue and tonsil tissues than in leukocytes (Leu.). (c) Relative expression level (mean \pm s.d.) of *SNRPN*. The data are normalized against *TBP*. SRS: an SRS patient with an epimutation (hypomethylation) of the *H19*-DMR; BWS1: a BWS patient with an epimutation (hypermethylation) of the *H19*-DMR; BWS2: a BWS patient with an epimutation (hypermethylation) of the *SNRPN*-DMR; PWS1: a Prader-Willi syndrome (PWS) patient with upd(15)mat; PWS2: a PWS patient with an epimutation (hypermethylation) of the *SNRPN*-DMR; AS1: an Angelman syndrome (AS) patient with upd(15)pat; and AS2: an AS patient with an epimutation (hypomethylation) of the *SNRPN*-DMR. The data were obtained using an ABI Prism 7000 Sequence Detection System (Applied Biosystems).

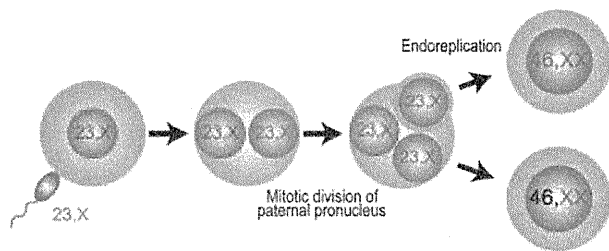


Figure 2 Schematic representation of the generation of the androgenetic/biparental mosaicism. Polar bodies are not shown.

one blastomere containing a paternally derived pronucleus and in the formation of the normal cell lineage by union of paternally and maternally derived pronuclei (Figure 2). This model has been proposed for androgenetic/biparental mosaicism generated after fertilization between a single ovum and a single sperm.^{5,15,16} The normal methylation pattern of the *XIST*-DMR is explained by assuming that the two X chromosomes in the androgenetic cell lineage undergo random X-inactivation, as in the normal cell lineage. Furthermore, the results of microsatellite analysis imply that the androgenetic cells were more prevalent in leukocytes than in tongue and tonsil tissues.

A somatic androgenetic cell lineage has been identified in seven liveborn patients including this patient (Supplementary Table 1).^{3–7} In this context, leukocytes are preferentially utilized for genetic analyses in human patients, and detailed examinations such as analyses of plural DMRs are necessary to detect an androgenetic cell lineage. Thus, the hitherto identified patients would be limited to those who had androgenetic cells as a predominant cell lineage in leukocytes probably because of a stochastic event and received detailed molecular studies. If so, an androgenetic cell lineage may not be so rare, and could be revealed by detailed analyses as well as examinations of additional tissues in patients with relatively complex phenotypes, as observed in the present patient.

Phenotypic features in androgenetic/biparental mosaicism would be determined by several factors. They include (1) the ratio of two cell lineages in various tissues/organs, (2) the number of imprinted domains relevant to specific features (for example, dysregulation of the imprinted domains on 11p15.5 and 14q32.2 is involved in placentomegaly^{9,17}), (3) the degree of clinical effects of dysregulated imprinted domains (an (epi)dominant effect has been assumed for the 11p15.5 imprinted domains¹⁸), (4) expression levels of imprinted genes in androgenetic cells (although *SNRPN* expression of this patient was consistent with androgenetic cells being predominant in leukocytes, complicated expression patterns have been identified for several imprinted genes in both androgenetic and parthenogenetic fetal mice, probably because of perturbed *cis*- and *trans*-acting regulatory mechanisms¹⁹) and (5) unmasking of possible paternally inherited recessive mutation(s) in androgenetic cells. Thus, in this patient, it appears that the extent of overall (epi)genetic aberrations exceeded the threshold level for the development of BWS-like and upd(14)pat-like body and placental phenotypes, but remained below

the threshold level for the occurrence of other imprinting disorders or recessive Mendelian disorders.

CONFLICT OF INTEREST

The authors declare no conflict of interest.

ACKNOWLEDGEMENTS

This work was supported by grants from the Ministry of Health, Labor, and Welfare, and the Ministry of Education, Science, Sports and Culture.

- Surani, M. A., Barton, S. C. & Norris, M. L. Development of reconstituted mouse eggs suggests imprinting of the genome during gametogenesis. *Nature* **308**, 548–550 (1984).
- McGrath, J. & Solter, D. Completion of mouse embryogenesis requires both the maternal and paternal genomes. *Cell* **37**, 179–183 (1984).
- Hoban, P. R., Heighway, J., White, G. R., Baker, B., Gardner, J., Birch, J. M. *et al.* Genome-wide loss of maternal alleles in a nephrogenic rest and Wilms' tumour from a BWS patient. *Hum. Genet.* **95**, 651–656 (1995).
- Bryke, C. R., Garber, A. T. & Israel, J. Evolution of a complex phenotype in a unique patient with a paternal uniparental disomy for every chromosome cell line and a normal biparental inheritance cell line. *Am. J. Hum. Genet.* **75**(Suppl), 831 (2004).
- Giurgea, I., Sanlaville, D., Fournet, J. C., Sempoux, C., Bellanne-Chantelot, C. & Touati, G. Congenital hyperinsulinism and mosaic abnormalities of the ploidy. *J. Med. Genet.* **43**, 248–254 (2006).
- Wilson, M., Peters, G., Bennetts, B., McGillivray, G., Wu, Z. H., Poon, C. *et al.* The clinical phenotype of mosaicism for genome-wide paternal uniparental disomy: two new reports. *Am. J. Med. Genet. Part A* **146A**, 137–148 (2008).
- Reed, R. C., Beischel, L., Schoof, J., Johnson, J., Raff, M. L. & Kapur, R. P. Androgenetic/biparental mosaicism in an infant with hepatic mesenchymal hamartoma and placental mesenchymal dysplasia. *Pediatr. Dev. Pathol.* **11**, 377–383 (2008).
- Jones, K. L. *Smith's Recognizable Patterns of Human Malformation* 6th edn. (Elsevier Saunders: Philadelphia, 2006).
- Kagami, M., Yamazawa, K., Matsubara, K., Matsuo, N. & Ogata, T. Placentomegaly in paternal uniparental disomy for human chromosome 14. *Placenta* **29**, 760–761 (2008).
- Kagami, M., Sekita, Y., Nishimura, G., Irie, M., Kato, F., Okada, M. *et al.* Deletions and epimutations affecting the human 14q32.2 imprinted region in individuals with paternal and maternal upd(14)-like phenotypes. *Nat. Genet.* **40**, 237–242 (2008).
- Yamazawa, K., Kagami, M., Nagai, T., Kondoh, T., Onigata, K., Maeyama, K. *et al.* Molecular and clinical findings and their correlations in Silver-Russell syndrome: implications for a positive role of IGF2 in growth determination and differential imprinting regulation of the IGF2-H19 domain in bodies and placentas. *J. Mol. Med.* **86**, 1171–1181 (2008).
- Weksberg, R., Shuman, C. & Beckwith, J. B. Beckwith-Wiedemann syndrome. *Eur. J. Hum. Genet.* **18**, 8–14 (2010).
- Yamazawa, K., Nakabayashi, K., Kagami, M., Sato, T., Saitoh, S., Horikawa, R. *et al.* Parthenogenetic chimaerism/mosaicism with a Silver-Russell syndrome-like phenotype. *J. Med. Genet.* **47**, 782–785 (2010).
- Ikari, K., Onda, H., Furushima, K., Maeda, S., Harata, S. & Takeda, J. Establishment of an optimized set of 406 microsatellite markers covering the whole genome for the Japanese population. *J. Hum. Genet.* **46**, 207–210 (2001).
- Kaiser-Rogers, K. A., McFadden, D. E., Livasy, C. A., Dansereau, J., Jiang, R., Knops, J. F. *et al.* Androgenetic/biparental mosaicism causes placental mesenchymal dysplasia. *J. Med. Genet.* **43**, 187–192 (2006).
- Kotzot, D. Complex and segmental uniparental disomy updated. *J. Med. Genet.* **45**, 545–556 (2008).
- Monk, D., Arnaud, P., Apostolidou, S., Hills, F. A., Kelsey, G., Stanier, P. *et al.* Limited evolutionary conservation of imprinting in the human placenta. *Proc. Natl. Acad. Sci. USA* **103**, 6623–6628 (2006).
- Azzi, S., Rossignol, S., Steunou, V., Sas, T., Thibaud, N., Danton, F. *et al.* Multilocus methylation analysis in a large cohort of 11p15-related foetal growth disorders (Russell Silver and Beckwith Wiedemann syndromes) reveals simultaneous loss of methylation at paternal and maternal imprinted loci. *Hum. Mol. Genet.* **18**, 4724–4733 (2009).
- Ogawa, H., Wu, Q., Komiya, J., Obata, Y. & Kono, T. Disruption of parental-specific expression of imprinted genes in uniparental fetuses. *FEBS Lett.* **580**, 5377–5384 (2006).

Supplementary Information accompanies the paper on Journal of Human Genetics website (<http://www.nature.com/jhg>)

ORIGINAL

GATA3 abnormalities in six patients with HDR syndrome

Maki Fukami¹⁾, Koji Muroya²⁾, Tetsuo Miyake^{1),3)}, Manami Iso¹⁾, Fumiko Kato¹⁾, Hisashi Yokoi⁴⁾, Yoshimi Suzuki⁵⁾, Koji Tsubouchi⁶⁾, Yoshiko Nakagomi⁷⁾, Nobuyuki Kikuchi⁸⁾, Reiko Horikawa⁹⁾ and Tsutomu Ogata¹⁾

¹⁾ Department of Molecular Endocrinology, National Research Institute for Child Health and Development, Tokyo 157-8535, Japan

²⁾ Department of Endocrinology and Metabolism, Kanagawa Children's Medical Center, Yokohama 232-8555, Japan

³⁾ Department of Pediatrics, St. Marianna University Hospital, Kawasaki 216-8511, Japan

⁴⁾ Department of Internal Medicine, Japanese Red Cross Nagoya First Hospital, Nagoya 453-8511, Japan

⁵⁾ Department of Pediatrics, Atsumi Hospital, Taiwara 441-3415, Japan

⁶⁾ Department of Pediatrics, Mino Municipal Hospital, Mino 501-3746, Japan

⁷⁾ Department of Pediatrics, Yamanashi University Hospital, Yamanashi 400-8510, Japan

⁸⁾ Department of Pediatrics, Yokohama City University Hospital, Yokohama 232-0024, Japan

⁹⁾ Division of Endocrinology and Metabolism, National Medical Center for Children and Mothers, Tokyo 157-8535, Japan

Abstract. *GATA3* mutations cause HDR (hypoparathyroidism, sensorineural deafness, and renal dysplasia) syndrome and, consistent with the presence of the second DiGeorge syndrome locus (*DGS2*) proximal to *GATA3*, distal 10p deletions often leads to HDR and DiGeorge syndromes. Here, we report on six Japanese patients with *GATA3* abnormalities. Cases 1–5 had a normal karyotype, and case 6 had a 46,XX,del(10)(p15) karyotype. Cases 1–6 had two or three of the HDR triad features. Case 6 had no DiGeorge syndrome phenotype except for hypoparathyroidism common to HDR and DiGeorge syndromes. Mutation analysis showed heterozygous *GATA3* mutations in cases 1–5, i.e., c.404–405insC (p.P135fsX303) in case 1, c.700T>C & c.708–709insC (p.F234L & p.S237fsX303) on the same allele in case 2, c.737–738insG (p.G246fsX303) in case 3, c.824G>T (p.W275L) in case 4, and IVS5+1G>C (splice error) in case 5. Deletion analysis of chromosome 10p revealed loss of *GATA3* and preservation of *D10S547* in case 6. The results are consistent with the previous finding that *GATA3* mutations are usually identified in patients with two or three of the HDR triad features, and provide supportive data for the mapping of *DGS2* in the region proximal to *D10S547*.

Key words: HDR syndrome, *GATA3*, DiGeorge syndrome, *DGS2*, Phenotypic spectrum

HDR (hypoparathyroidism, sensorineural deafness, and renal dysplasia) syndrome is an autosomal dominant disorder first reported by Bilous *et al.* [1]. This condition is primarily caused by haploinsufficiency of *GATA3* on chromosome 10p15, although *GATA3* mutations have not been identified in a small portion of patients with clinical features compatible with HDR syndrome [2, 3]. *GATA3* consists of six exons, and encodes a transcription factor with two transactivating domains and two zinc finger domains on exons 2–6

[2]. *GATA3* is expressed in the developing parathyroid glands, inner ears, and kidneys, together with thymus and central nervous system (CNS) [4, 5].

Distal 10p deletions involving *GATA3* often lead to DiGeorge syndrome associated with hypoplastic thymus, T-cell immunodeficiency, hypoparathyroidism, congenital cardiac defects, and facial dysmorphism, in addition to HDR syndrome [6, 7]. Thus, deletion mappings have been performed, localizing the second DiGeorge syndrome locus (*DGS2*) to a ~1 cM region proximal to *D10S547* (the locus order: 10pter–*GATA3*–*D10S547*–*DGS2*–10cen) [6, 7].

Here, we report clinical and molecular findings in five patients with intragenic *GATA3* mutations and one patient with distal 10p deletion involving *GATA3*, and discuss the clinical features in *GATA3* mutation posi-

Received Aug. 4, 2010; Accepted Dec. 16, 2010 as K10E-234

Released online in J-STAGE as advance publication Jan. 13, 2011

Correspondence to: Tsutomu Ogata, Department of Molecular Endocrinology, National Research Institute for Child Health and Development, 2-10-1 Okura Setagaya-ku, Tokyo 157-8535, Japan. E-mail: tomogata@nch.go.jp

©The Japan Endocrine Society

Table 1 Summary of six patients with *GATA3* mutation or deletion

	Case 1	Case 2	Case 3	Case 4	Case 5	Case 6
Present age	40 years	39 years	4 years	31 years	17 years	4 years
Sex	Female	Female	Male	Female	Male	Female
Karyotype	46,XX	46,XX	46,XY	46,XX	46,XY	46,XX,del(10)(p15)
Hypoparathyroidism	Yes	Yes	Yes	Yes	Yes	Yes
Symptom	Convulsion	Tetany	No ^b	Convulsion	Convulsion	Convulsion
Ca (mg/dL)	3.4	3.4	2.7	4.3	3.0	4.7
P (mg/dL)	8.0	7.9	8.1	7.9	8.7	8.6
Intact PTH (pg/mL)	Undetected	Undetected	14	Undetected	Undetected	15
Age at diagnosis	10 years	13 years	17 months	3 years	17 months	2 weeks
Sensorineural deafness	Yes	Yes	No	Yes	Yes	Yes
Hearing level (dB) ^a	50 (B)	>70 (B)	Normal	60 (B)	50 (B)	90 (B)
Age at diagnosis	13 years	6 years		11 years	12 months	6 months
Renal lesion	Yes	Yes	Yes	Equivocal ^c	Yes	Yes
Malformation	RH (L)	PCD (B)	PD (R)	Absent	RH (L)	VUR (B)
Age at diagnosis	9 years	27 years	17 months		17 months	2 months

Abbreviations: PTH, parathyroid hormone; dB, decibel; B, bilateral; L, left; R, right; RH, renal hypoplasia; PCD, pelvicalyceal deformity; PD, pelvic duplication; and VUR, vesicoureteral reflux.

^a Degree of hearing loss: normal, <25 dB; mild 26–40 dB; moderate 41–55 dB; moderately severe, 56–70 dB; and profound, >90 dB.

^b Hypocalcemia was revealed by routine biochemical studies, when this boy was admitted because of bronchopneumonia.

^c Renal malformation was absent, but renal dysfunction with increased serum creatinine was noticed during pregnancy.

Normal reference data: Ca: 8.84–10.44 mg/dL; P: 4.5–6.5 mg/dL; and intact PTH: 10–65 pg/mL.

five patients and the chromosomal location of *DGS2*.

Patients and Methods

Patients

We studied six hitherto unreported Japanese patients (cases 1–6) with two or three HDR triad features. Cases 1–5 had a normal karyotype, and case 6 had a 46,XX,del(10)(p15) karyotype. Cases 1–4 and 6 were apparently sporadic cases, whereas case 5 was a possible familial case: the father received renal dialysis due to chronic renal failure from his twenties, and the paternal grandmother had unilateral renal hypoplasia, although they lacked clinical features suggestive of hypoparathyroidism and hearing difficulty.

Clinical phenotypes of the HDR triad features are summarized in Table 1. Hypoparathyroidism was noticed by convulsion in cases 1 and 4–6 and by tetany in case 2; in case 3, it was incidentally found by biochemical examinations at the time of admission due to bronchopneumonia. After confirming parathyroid hormone deficiency, 1 α (OH) vitamin D therapy was started, successfully normalizing serum calcium and phosphate values in cases 1–6. Sensorineural deafness was demonstrated in cases 1, 2, and 4–6 by auditory brainstem response or audiometry, and they required

hearing aids in their daily life. Case 3 had no hearing difficulty with normal auditory brainstem response. Renal lesion was radiologically confirmed in cases 1–3, 5, and 6. Although case 4 had no discernible renal malformation, she manifested renal dysfunction during pregnancy. In addition, case 6 exhibited developmental delay but lacked hypoplastic thymus, T-cell immunodeficiency, congenital cardiac defects, and facial dysmorphism characteristic of DiGeorge syndrome.

Mutation analysis of *GATA3*

This study was approved by the Institutional Review Board Committee at National Center for Child Health and Development. After obtaining informed consent, leukocyte genomic DNA samples of cases 1–6 were amplified by PCR for the coding regions on exons 2–6 and their flanking splice sites, and the PCR products were subjected to direct sequencing from both directions on a CEQ 8000 autosequencer (Beckman Coulter, Fullerton, CA). The primer sequences and the PCR conditions were as described previously [2, 3]. To confirm a heterozygous mutation, the corresponding PCR products were subcloned with a TOPO TA Cloning Kit (Life Technologies, Carlsbad, CA), and normal and mutant alleles were sequenced separately.

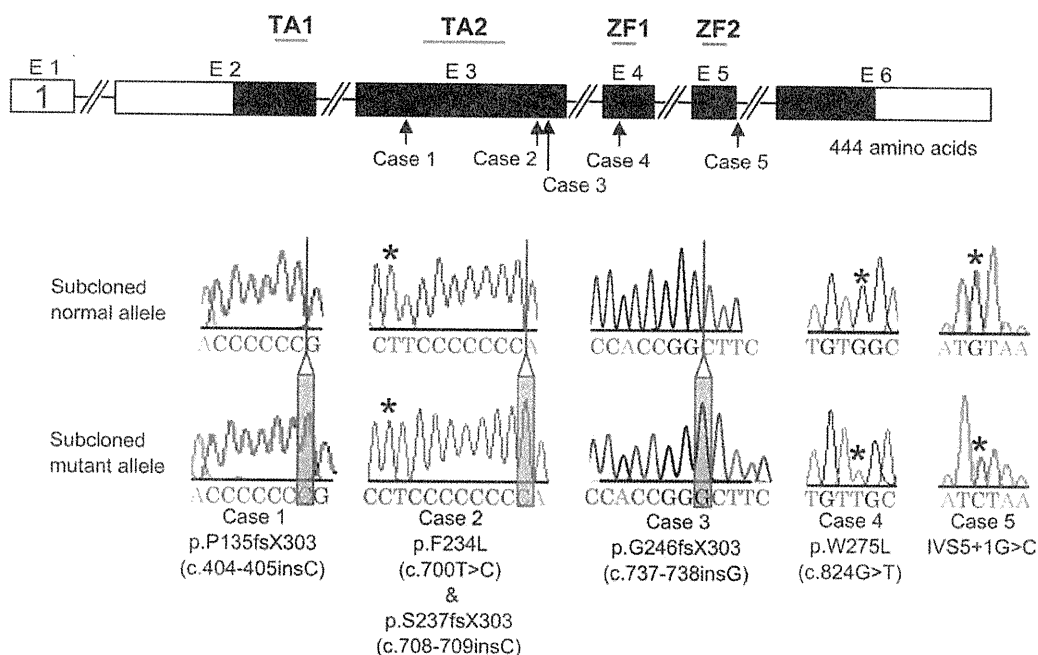


Fig. 1 Mutation analysis of *GATA3*.

Upper part: The structure of *GATA3* and the position of the mutations identified in cases 1–5. *GATA3* consists of exons 1–6 (E1–E6) and encodes two transactivating domains (TA1 and TA2) and two zinc finger domains (ZF1 and ZF2). The black and white boxes denote the coding regions and the untranslated regions, respectively.

Lower part: Electrochromatograms showing the subcloned normal and mutant sequences in cases 1–5.

Deletion analysis of 10p

To indicate an extent of the 10p deletion in case 6, oligoarray comparative genomic hybridization (CGH) was carried out with 1x244K Human Genome Array (catalog No. G4411B) (Agilent Technologies, Palo Alto, CA), according to the manufacturer's protocol. Furthermore, fluorescence *in situ* hybridization (FISH) was performed with an RP11-554F11 BAC probe containing the whole *GATA3* gene [3] and an RP11-17E09 BAC probe containing *D10S547* (BACPAC Resources Center, Oakland, CA), together with a CEP 10 probe for *D10Z1* (Abbott, Chicago, IL) utilized as an internal control. The two BAC probes were labeled with digoxigenin and detected by rhodamine anti-digoxigenin, and the control probe was detected according to the manufacturer's protocol.

Results

Mutation analysis of *GATA3*

Direct sequencing identified heterozygous *GATA3* mutations in cases 1–5, i.e., a frameshift mutation (c.404–405insC, p.P135fsX303) in case 1, a mis-

sense mutation (c.700T>C, p.F234L) and a frameshift mutation (c.708–709insC, p.S237fsX303) on the same allele in case 2, a frameshift mutation (c.737–738insG, p.G246fsX303) in case 3, a missense mutation (c.824G>T, p.W275L) in case 4, and a splice donor site mutation (IVS5+1G>C) in case 5 (Fig. 1). Unfortunately, the renal phenotype positive father and paternal grandmother of case 5 were not examined. These mutations were absent from 200 control subjects. No intragenic mutation was identified in case 6 with distal 10p deletion.

Deletion analysis of 10p

CGH revealed a ~10 Mb terminal deletion from chromosome 10p of case 6 (Fig. 2). FISH analysis showed that the 10p deletion chromosome was missing *GATA3* and retained *D10S547*.

Discussion

Cases 1–6 had two or three of the HDR triad features and heterozygous *GATA3* abnormalities. This is consistent with the previous notion that *GATA3* mutations

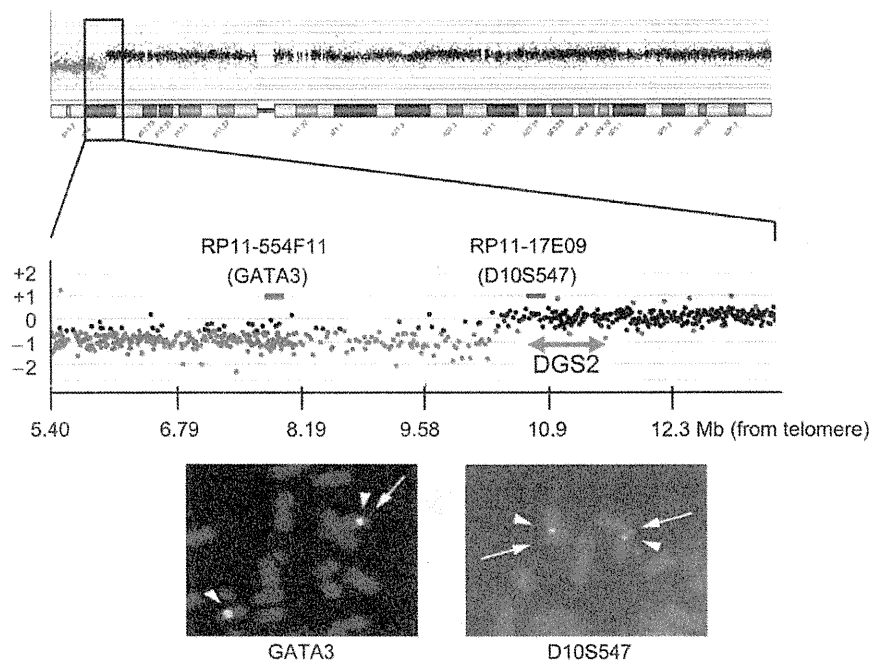


Fig. 2 Deletion analysis of 10p. The green and black signals in CGH indicate the deleted and preserved regions on the 10p deleted chromosome, respectively. The critical region for *DGS2* is indicated. The RP11-554F11 probe containing *GATA3* detects only a single signal (an arrow), whereas the RP11-17E09 probe containing *D10S547* identifies two signals (arrows). The arrowheads indicate *D10Z1* detected by a control CEP 10 probe.

are usually identified in patients with two or three of the HDR triad features [8, 9]. However, this would more or less be due to an ascertainment bias that *GATA3* are usually examined in patients diagnosed as having HDR syndrome. Indeed, familial studies of probands with typical HDR syndrome have identified *GATA3* mutations in subjects with apparently deafness only phenotype [3, 10], although there has been no report documenting apparently normal phenotype in individuals with *GATA3* mutations. It is possible, therefore, that *GATA3* mutations are associated with a relatively wide penetrance and expressivity of the HDR triad features. In this context, it is notable that the father and the paternal grandmother of case 5 had renal abnormalities as the sole discernible clinical phenotype. This suggests that *GATA3* mutations may cause renal abnormalities alone in exceptional patients, although mutations

analysis could not be performed for the father and the grandmother.

Case 6 lacked T-cell immunodeficiency, congenital cardiac defects, and abnormal facial appearance characteristic of DiGeorge syndrome. While case 6 had hypoparathyroidism, this is explained by loss of *GATA3*. In addition, developmental delay is ascribed to chromosome aberration. Thus, genotype-phenotype correlation in case 6 is consistent with the previous mapping of *DGS2* to a region proximal to *D10S547* [6, 7].

Acknowledgements

This work was supported by Grants for Child Health and Development and for Research on Children and Families from the Ministry of Health, Labor, and Welfare.

References

1. Bilous RW, Murty G, Parkinson DB, Thakker RV, Coulthand MG, Burn J, Mathias D, Kendall-Taylor P (1992) Autosomal dominant familial hypoparathyroidism, sensorineural deafness, and renal dysplasia. *N Engl J Med* 327: 1069–1074.
2. Van Esch H, Groenen P, Nesbit MA, Schuffenhauer S,

- Lichtner P, Vanderlinden G, Harding B, Beetz R, Bilous RW, Holdaway I, Shaw NJ, Fryns JP, Van de Ven W, Thakker RV, Devriendt K (2000) GATA3 haplo-insufficiency causes human HDR syndrome. *Nature* 406: 419–422.
3. Muroya K, Hasegawa T, Ito Y, Nagai T, Isotani H, Iwata Y, Yamamoto K, Fujimoto S, Seishu S, Fukushima Y, Hasegawa Y, Ogata T (2001) GATA3 abnormalities and the phenotypic spectrum of HDR syndrome. *J Med Genet* 38: 374–380.
 4. Labastie MC, Catala M, Gregoire JM, Peault B (1995) The GATA3 gene is expressed during human kidney embryogenesis. *Kidney Int* 47: 1597–1603.
 5. Debacker C, Catala M, Labastie MC (1999) Embryonic expression of the human GATA3 gene. *Mech Dev* 85: 183–187.
 6. Schuffenhauer S, Lichtner P, Peykar-Derakhshandeh P, Murken J, Haas OA, Back E, Wolff G, Zabel B, Barisic I, Rauch A, Borochowitz Z, Dallapiccola B, Ross M, Meitinger T (1998) Deletion mapping on chromosome 10p and definition of a critical region for the second DiGeorge syndrome locus (DGS2). *Eur J Hum Genet* 6: 213–225.
 7. Lichtner P, König R, Hasegawa T, Van Esch H, Meitinger T, Schuffenhauer S (2000) An HDR (hypoparathyroidism, deafness, renal dysplasia) syndrome locus maps distal to the DiGeorge syndrome region on 10p13/14. *J Med Genet* 37: 33–37.
 8. Nesbit MA, Bowl MR, Harding B, Ali A, Ayala A, Crowe C, Dobbie A, Hampson G, Holdaway I, Levine MA, McWilliams R, Rigden S, Sampson J, Williams AJ, Thakker RV (2004) Characterization of GATA3 mutations in the hypoparathyroidism, deafness, and renal dysplasia (HDR) syndrome. *J Biol Chem* 279: 22624–22634.
 9. Ali A, Christie PT, Grigorieva IV, Harding B, Van Esch H, Ahmed SF, Bitner-Glindzicz M, Blind E, Bloch C, Christin P, Clayton P, Gecz J, Gilbert-Dussardier B, Guillen-Navarro E, Hackett A, Halac I, Hendy GN, Lalloo F, Mache CJ, Mughal Z, Ong AC, Rinat C, Shaw N, Smithson SF, Tolmie J, Weill J, Nesbit MA, Thakker RV (2007) Functional characterization of GATA3 mutations causing the hypoparathyroidism-deafness-renal (HDR) dysplasia syndrome: insight into mechanisms of DNA binding by the GATA3 transcription factor. *Hum Mol Genet* 16: 265–275.
 10. Chiu WY, Chen HW, Chao HW, Yann LT, Tsai KS (2006) Identification of three novel mutations in the GATA3 gene responsible for familial hypoparathyroidism and deafness in the Chinese population. *J Clin Endocrinol Metab* 91: 4587–4592.

Proximal Promoter of the Cytochrome P450 Oxidoreductase Gene: Identification of Microdeletions Involving the Untranslated Exon 1 and Critical Function of the SP1 Binding Sites

Shun Soneda,* Takashi Yazawa,* Maki Fukami,* Masanori Adachi, Michiyo Mizota, Kenji Fujieda, Kaoru Miyamoto, and Tsutomu Ogata

Department of Molecular Endocrinology (S.S., M.F., T.O.), National Research Institute for Child Health and Development, Tokyo 157-8535, Japan; Department of Pediatrics (S.S.), St. Marianna University School of Medicine, Kawasaki 216-8511, Japan; Department of Biochemistry, Faculty of Medical Sciences (T.Y., K.M.), University of Fukui, Fukui 910-1193, Japan; Division of Endocrinology and Metabolism (M.A.), Kanagawa Children's Medical Center, Yokohama 232-8555, Japan; Department of Pediatrics (M.M.), Kagoshima University School of Medicine, Kagoshima 890-8520, Japan; Department of Pediatrics (K.F.), Asahikawa Medical Collage, Asahikawa 078-8510, Japan; and Department of Pediatrics (T.O.), Hamamatsu University School of Medicine, Hamamatsu 431-3192, Japan

Context: *POR* (cytochrome P450 oxidoreductase) is a ubiquitously expressed gene encoding an electron donor to all microsomal P450 enzymes and several non-P450 enzymes. *POR* mutations cause an autosomal recessive disorder characterized by skeletal dysplasia, adrenal dysfunction, and disorders of sex development. Although recent studies have indicated the presence of a CpG-rich region characteristic of housekeeping genes around the untranslated exon 1 (exon 1U) and a tropic effect of thyroid hormone on *POR* expression via thyroid hormone receptor- β , detailed regulatory mechanisms for the *POR* expression remain to be clarified.

Objective: Our objective was to report a pivotal element of the proximal promoter of *POR*.

Results: We first studied three patients (cases 1–3) with *POR* deficiency due to compound heterozygosity with an p.R457H mutation and transcription failure of an apparently normal allele, by oligoarray comparative genomic hybridization and serial direct sequencing of the deletion fusion points. Consequently, a 2,487-bp microdeletion involving exon 1U was identified in case 1 and an identical 49,604-bp deletion involving exon 1U and exon 1 was found in cases 2 and 3. We next analyzed the 2,487-bp region commonly deleted in cases 1–3 by *in silico* analysis, DNA binding analysis, luciferase assays, and methylation analysis. The results showed a critical function of the evolutionally conserved SP1 binding sites just upstream of exon 1U, especially the binding site at the position –26/–17, in the transcription of *POR*.

Conclusions: The results suggest that the SP1 binding sites constitute an essential element of the *POR* proximal promoter. (*J Clin Endocrinol Metab* 96: E1881–E1887, 2011)

Cytochrome P450 (CYP) oxidoreductase (*POR*) deficiency (*PORD*) is a rare autosomal recessive disorder caused by mutations in the gene encoding a flavoprotein that functions as an electron donor to all microsomal P450 enzymes and several non-P450 enzymes (1–3). Salient clin-

ical features of *PORD* include skeletal dysplasia referred to as Antley-Bixler syndrome, adrenal dysfunction, 46,XY and 46,XX disorders of sex development (*DSD*), and maternal virilization during pregnancy (1–4). Such features are primarily explained by impaired activities of *POR*-

ISSN Print 0021-972X ISSN Online 1945-7197
Printed in U.S.A.

Copyright © 2011 by The Endocrine Society

doi: 10.1210/jc.2011-1337 Received April 25, 2011. Accepted August 18, 2011.

First Published Online September 7, 2011

* S.S., T.Y., and M.F. contributed equally to this work.

Abbreviations: CGH, Comparative genomic hybridization; CYP, cytochrome P450; *DSD*, disorders of sex development; exon 1U, untranslated exon 1; HEK, human embryonic kidney; *POR*, CYP oxidoreductase; *PORD*, *POR* deficiency; SL2, Schneider line 2.

dependent CYP51A1 and squalene epoxidase involved in cholesterologenesis and CYP17A1, CYP21A2, and CYP19A1 involved in steroidogenesis (1–4). Anorectal and urinary anomalies are also occasionally observed in PORD, probably due to decreased activity of CYP26 relevant to retinoic acid metabolism (5). The complete absence of *POR* activity is assumed to be lethal (4), and consistent with this, all the patients identified to date have at least one missense mutation that is likely to preserve some residual activity (1, 2, 6, 7). In addition, heterozygosity with one apparently normal allele has been reported in approximately 12% of PORD patients (4).

The *POR/por* gene is transcribed ubiquitously with more or less variable expression levels among different tissues (8, 9). Consistent with the ubiquitous expression pattern, rat *Por* is known to be associated with a CpG-rich region (CpG islands) (9) characteristic of housekeeping genes (10). Similarly, human *POR* consists of a single untranslated exon 1 (exon 1U) and coding exons 1–15, and the region around exon 1U harbors a CpG-rich region (11). In addition, the SP1 binding sites as a potential proximal promoter element reside in the CpG-rich region of rat *Por* (9), whereas they have not yet been reported in the CpG-rich region of human *POR*. Furthermore, Tee *et al.* (12) have recently studied the approximately 300-bp

proximal promoter region just upstream of exon 1U of human *POR*, showing that thyroid hormone exerts a major trophic effect on *POR* expression primarily via thyroid hormone receptor- β , with thyroid hormone receptor- α , estrogen receptor- α , Smad3, and Smad4 exerting lesser modulatory effects. However, the detailed regulatory mechanisms for the transcription of human *POR* remain to be clarified.

Here, we report two types of microdeletions, one involving exon 1U alone and the other involving exon 1U and exon 1, in patients with PORD and suggest a pivotal role of the SP1 binding sites in the transcriptional regulation of *POR*. The results, in conjunction with the previous data (12), provide significant progress in the clarification of the regulatory machinery for the expression of *POR*.

Patients and Methods

Patients

We examined three nonconsanguineous patients (case 1 with 46,XY and cases 2 and 3 with 46,XX) reported in our previous paper describing 35 patients with PORD (7); cases 1, 2, and 3 in this report correspond to cases 18, 26, and 27 in the previous paper, respectively. Cases 1–3 manifested Antley-Bixler syndrome-compatible skeletal features, adrenal dysfunction with

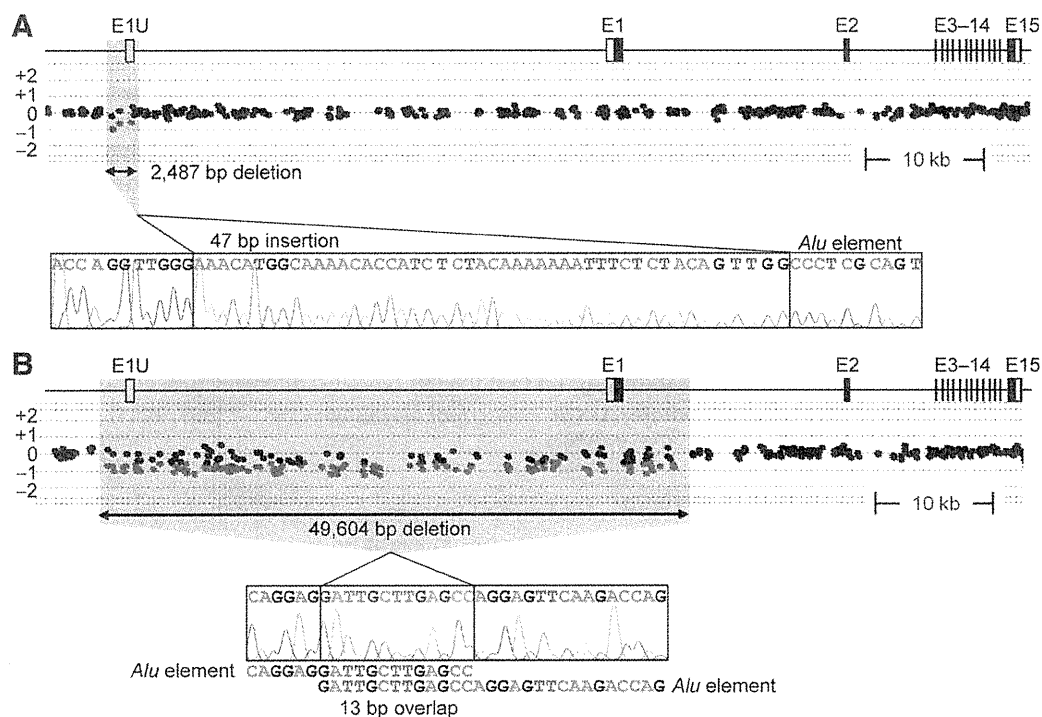


FIG. 1. Identification and characterization of the microdeletions in case 1 (panel A) and cases 2 and 3 (panel B) by CGH analysis and direct sequencing of the deletion junctions. The position of *POR* exons (E1U–E15) is shown on the CGH findings; the *black and white boxes* denote the coding regions and the untranslated regions, respectively. In the CGH results, the *black and green dots* denote signals indicative of the normal and the decreased (<-0.5) copy numbers, respectively. In the direct sequencing findings, the 47-bp segment inserted into the fusion point in case 1 is *highlighted with light yellow*, and the 13-bp overlapping sequence at the fusion point in cases 2 and 3 is *highlighted with light blue*. The *Alu* elements are indicated with *light blue bars*.

drastically compromised cortisol response to ACTH stimulation, and DSD (bilateral cryptorchidism in case 1, partial labial fusion in case 2, and mild clitoromegaly in case 3). Cases 2 and 3 also experienced adrenal crisis, whereas maternal virilization during pregnancy was not identified in cases 1–3. In addition, case 2 had right vesicoureteral reflux, and case 3 manifested imperforated anus. In cases 1–3, direct sequencing for leukocyte genomic DNA indicated apparent heterozygosity for the Japanese founder mutation p.R457H, and that for leukocyte cDNA demonstrated transcription failure of an apparently normal allele (7). Thus, although cases 1–3 were found to have compound heterozygosity for p.R457H and transcription failure, the cause of transcription failure remained to be clarified.

Primer and probe

The primers and probes used in the present study are shown in Supplemental Table 1 (published on The Endocrine Society's Journals Online web site at <http://endo.endojournals.org>).

Genome structure analysis

Oligoarray comparative genomic hybridization (CGH) was performed for leukocyte genomic DNA, using a custom-build oligo-microarray containing 39,169 probes for an approximately 8-Mb region around *POR* and 26,662 reference probes for a different genomic interval (2x105K format, design ID 022431) (Agilent Technologies, Palo Alto, CA). The procedure

was as described in the manufacturer's instructions. To determine the deletion size and the junction structure, serial direct sequencing was performed for long PCR products obtained with primer pairs flanking the deleted region, and the obtained junction sequence was compared with the reference sequence at the NCBI Database (NT_007933.15). The presence or absence of repeat sequences around the breakpoints was examined with Repeatmasker (<http://www.repeatmasker.org>).

In silico analysis

In silico analysis was performed for CpG islands, evolutionarily conserved sequences, and promoter-associated histone marks, using UCSC genome browser (<http://genome.ucsc.edu/>). Putative transcription factor binding sites were searched by TFSEARCH (<http://mbs.cbrc.jp/research/db/TFSEARCH.html>). In addition, because animal *Por* has been well studied in rats (9), conservation status of identified sites was examined using rat data. The transcription start site of *POR* exon 1U (+1) was determined on the basis of the *POR* cDNA sequence (NM_000941) obtained from the NCBI database.

Luciferase assays

A series of promoter-reporter constructs were generated by inserting PCR-amplified DNA fragments into PGL3-enhancer vector or pGL3-basic vector (Promega, Madison, WI). Deletion mutants were created by site-directed mutagenesis. Transient transfection was carried out using human embryonic kidney (HEK) 293 cells with endogenous SP families, because of their stable transfection efficiency and usefulness in *in vitro* functional studies for SP1 binding sites (13). HEK 293 cells were cultured in DMEM at 37 C, seeded in 12-well dishes, and transfected using Lipofectamine 2000 (Life Technologies, Carlsbad, CA) with 0.6 μ g of the reporter plasmids. As an internal control for the transfection, 20 ng pRL-CMV vector (Promega) was used. In addition, transient transfection was also performed using *Drosophila* Schneider line 2 (SL2) cells (CRL-1963; American Type Culture Collection, Manassas, VA) that lack endogenous SP families. SL2 cells were grown in Schneider's medium at 25 C, seeded in six-well dishes, and transfected using calcium phosphate (14) with 1.0 μ g of the reporter plasmid and a total of 50 ng of various combinations of the SP1 expression vector (pPAC-SP1) and an empty pPAC vector (pPAC-SP3). As an internal control for the transfection, 50 ng pPAC- β -galactosidase vector was used. For both experiments using HEK 293 cells and SL2 cells, luciferase activities were determined at 48 h after the transfections.

Transfections were performed in triplicate within a single experiment, and the experiments were repeated three times. The results are expressed as mean \pm SEM, and statistical significance was examined by the *t* test. $P < 0.05$ was considered significant.

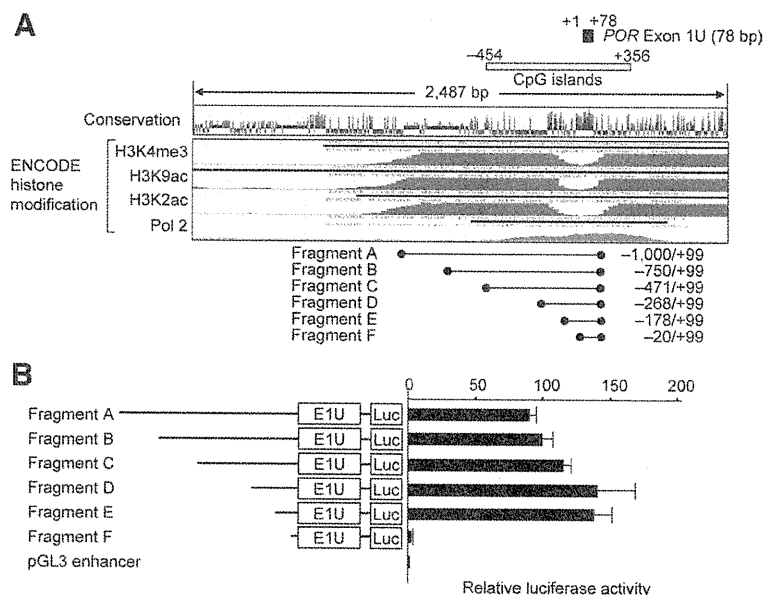


FIG. 2. Localization of the promoter region to a 178-bp segment just upstream of exon 1U. Panel A, *In silico* analysis in search of the promoter-compatible sequences. The transcription start site of *POR* exon 1U (+1) is based on the *POR* cDNA sequence at the NCBI database (NM_000941). The CpG-rich region spans from -454 to $+356$ bp. The ENCODE histone modification analysis indicates the presence of a highly conserved promoter-compatible sequence just upstream of exon 1U. The fragments A–F denote the DNA sequences used for the luciferase assays. Panel B, Luciferase reporter assays using the fragments A–F. The results are expressed as fold-change of the target vectors over the empty pGL3 enhancer vector (mean \pm SEM). Transfections were performed in triplicate within a single experiment, and the experiments were repeated three times. Although the increase in the relative luciferase activity is significant for fragment A (92.6 ± 5.2 , $P = 0.0006$), fragment B (101.6 ± 5.8 , $P = 0.0006$), fragment C (106.0 ± 5.5 , $P = 0.0004$), fragment D (137.7 ± 29.0 , $P = 0.0009$), and fragment E (131.3 ± 13.4 , $P = 0.0006$), it is not significant for fragment F (2.6 ± 1.1 , $P = 0.25$).

DNA binding analysis

EMSA was performed as described previously (15). In brief, 10 μg of nuclear extracts of HEK 293 cells were incubated with ³²P-labeled oligonucleotides and unlabeled polydeoxyinosinic-deoxycytidylic acids and subjected to polyacrylamide gel electrophoresis (4%). For a competition experiment, a 200-fold molar excess of unlabeled competitor DNA was added. Supershift assay was performed by preincubating the nuclear extracts with anti-SP1 antisera (PEP2) and/or anti-SP3 antisera (D-20) (Santa Cruz Biotechnology, Santa Cruz, CA).

Methylation analysis

Bisulfite sequencing was performed for human leukocyte- and HEK 293-derived genomic DNA samples treated with the EZ DNA Methylation Kit (Zymo Research, Orange, CA) that converts all the cytosines except for methylated cytosines at the CpG dinucleotides into uracils and subsequently thymines. A 282-bp CpG-rich region containing SP1 binding sites just upstream of exon 1U was amplified with primer sets that hybridize to both methylated and unmethylated alleles because of absent CpG dinucleotides within the primer sequences. Subsequently,

the PCR products were subcloned with the TOPO TA Cloning Kit (Life Technologies), and multiple clones were subjected to direct sequencing on the CEQ 8000 autosequencer (Beckman Coulter, Fullerton, CA).

Results

Identification and characterization of microdeletions in cases 1–3

Oligoarray CGH analysis indicated cryptic heterozygous deletions in cases 1–3 (Fig. 1). Furthermore, sequencing of the long PCR products harboring the fusion points revealed a 2,487-bp microdeletion (13,575,403–13,577,889 bp) encompassing exon 1U in case 1 and an identical 49,604-bp deletion (13,571,326–13,620,929 bp) involving exon 1U and exon 1 in cases 2 and 3. Thus, the 2,487-bp microdeletion on the noncoding upstream region was common to cases 1–3. The microdeletion in case

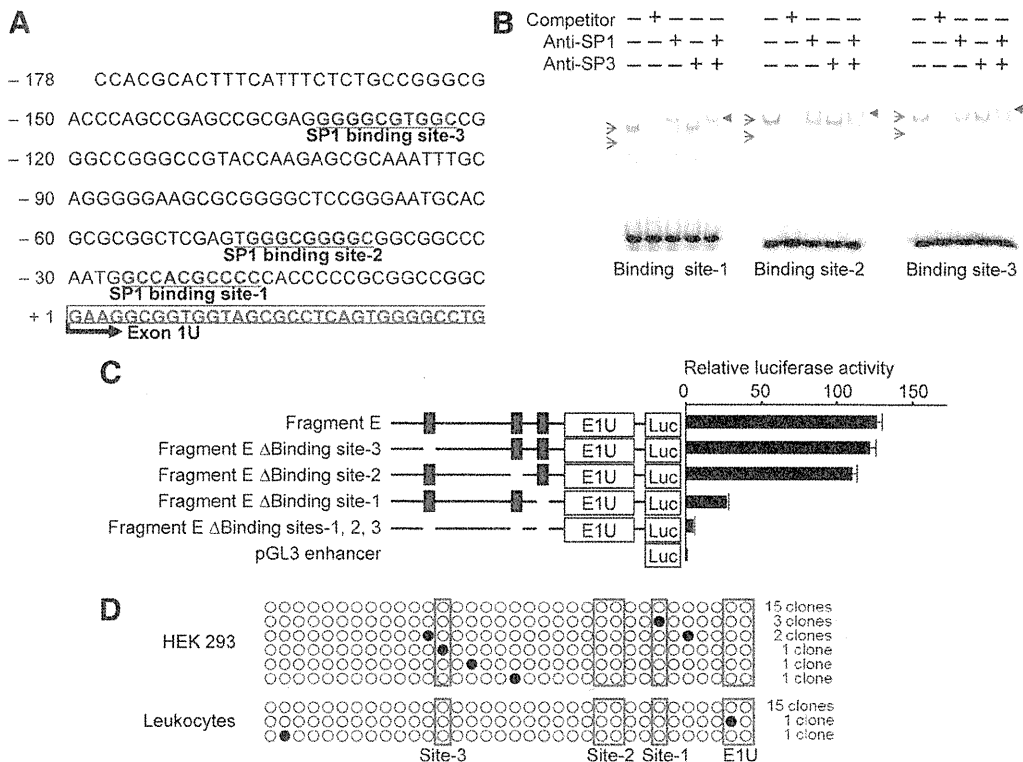


FIG. 3. Functional studies of the SP1 binding sites. Panel A, The three potential SP1 binding sites 1–3 at the position just upstream of exon 1U. The transcription start site of *POR* exon 1U (+1) is based on the *POR* cDNA sequence at the NCBI database (NM_000941). Panel B, EMSA showing positive bindings of SP1 and SP3 proteins to the SP1 binding sites 1–3. The red arrows indicate the strong bands derived from the SP1 protein binding to the probes containing the SP1 binding sites. These bands become weak, and supershifted bands (red arrowheads) are seen by adding anti-SP1. In addition, the blue arrows denote specific bands derived from the SP3 protein binding to the same probes. These bands become very weak by adding anti-SP3; the extremely faint supershifted bands are not visible in this figure. The band shift pattern is more obvious for SP1 protein than for SP3 protein. Panel C, Luciferase reporter assays using fragment E and its deletion mutants. The results are expressed as fold change of the target vectors over the empty pGL3 enhancer vector (mean ± SEM). Transfections were performed in triplicate within a single experiment, and the experiments were repeated three times. Although the relative luciferase activity is similar between Fragment E (121.8 ± 3.4) and ΔBinding site-3 (117.8 ± 3.1) ($P = 0.22$), it is significantly different between Fragment E and ΔBinding site-2 (105.7 ± 3.5) ($P = 0.015$), ΔBinding site-1 (25.8 ± 1.2) ($P = 0.0007$), and ΔBinding site-1, -2, and -3 (5.2 ± 0.5) ($P = 0.0004$). Panel D, Methylation analysis of the CpG-rich region. Each circle denotes a CpG island, and filled and open circles represent methylated and unmethylated cytosines, respectively. The CpG dinucleotides within the exon 1U are surrounded by blue squares, and those within the SP1 binding sites 1, 2, and 3 by red squares.

1 occurred between an *Alu* element and a nonrepeat sequence and was associated with an addition of a 47-bp segment of unknown origin, whereas that in cases 2 and 3 occurred between two *Alu* elements with an overlap of a 13-bp segment.

Critical function of the SP1 binding sites

In silico analysis for the noncoding 2,487-bp region showed an 810-bp long CpG-rich region involving exon 1U, an approximately 350-bp long evolutionally conserved sequence-rich region encompassing exon 1U, and an approximately 1.3-kb region with promoter-associated histone marks (Fig. 2A). The TATA box was not identified. Thus, relative luciferase activity was examined for fragments A–F with various lengths of the candidate promoter region, localizing a critical sequence for the *POR* promoter to a 178-bp segment defined by fragment E and fragment F (Fig. 2B).

The 178-bp segment was found to harbor three SP1 binding sites, *i.e.* site 1 at the position –26/–17, site 2 at the position –48/–39, and site 3 at the position –132/–123 (Fig. 3A). The three binding sites were well conserved in rats. EMSA indicated specific binding of SP1 and SP3 proteins to the three binding sites, with the band shift pattern being more obvious for SP1 protein than for SP3 protein (Fig. 3B). Deletion of the binding site 1 and the binding site 2 significantly reduced the relative luciferase activity (by ~80 and ~15%, respectively), although deletion of the binding site 3 had no significant effect on the relative luciferase activity; furthermore, loss of the binding sites 1–3 virtually abolished the relative luciferase activity (Fig. 3C). The 282-bp segment containing the three SP1 binding sites was almost completely unmethylated (Fig. 3D).

Furthermore, relative luciferase activity was examined for a 170-bp fragment (–120/+50) harboring the SP1 binding site 1 and the SP1 binding site 2, using SL2 cells devoid of endogenous SP families. Relative luciferase activity was clearly increased in a dose-dependent manner by adding the *SP1* expression vector but was barely elevated by adding the *SP3* expression vector (Fig. 4).

Discussion

We identified two types of cryptic deletions, one involving exon 1U alone and the other encompassing exon 1U and exon 1, in three cases with PORD. The microdeletion in case 1 is explained by nonhomologous end joining that occurs between nonhomologous sequences and is frequently accompanied by an insertion of a short segment at the fusion point (16). The microdeletion in cases 2 and 3 is compatible with a repeat sequence mediated nonallelic

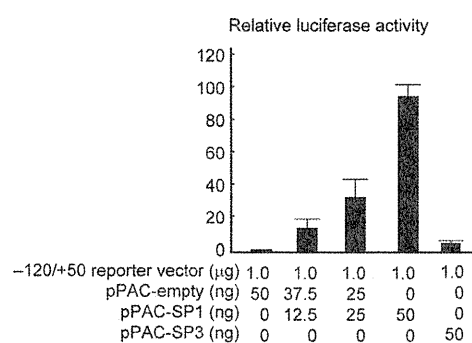


FIG. 4. Luciferase assays of a fragment containing the SP1 binding sites 1 and 2, using SL2 cells lacking endogenous SP families. The results are expressed as fold change of the target vectors over the empty pPAC vector (mean ± SEM). Transfections were performed in triplicate within a single experiment, and the experiments were repeated three times. The relative luciferase activity is significantly increased by adding the *SP1* expression vector of 12.5 ng (14.7 ± 4.4) ($P = 0.037$), 25.0 ng (31.8 ± 7.6) ($P = 0.035$), and 50 ng (95.8 ± 7.1) ($P = 0.0002$), although it is barely elevated by adding the *SP3* expression vector of 50 ng (5.2 ± 1.5) ($P = 0.054$).

intrachromosomal or interchromosomal recombination (16). Although cases 2 and 3 were apparently nonconsanguineous, it would not be unexpected that the same repeat-mediated genomic rearrangement took place in unrelated individuals. Notably, because the apparently normal allele in cases 1–3 was not transcribed (7), this implies that the 2,487-bp microdeletion common to cases 1–3 has affected the promoter function for *POR*. In this context, because approximately 12% of patients with PORD are known to be heterozygotes with one apparently normal *POR* allele (4), it might be possible that some, if not all, of them have similar microdeletions or other genetic aberrations affecting the *POR* transcription.

The present study revealed a pivotal role of the SP1 binding sites, especially the binding site 1, in the transcription of *POR*. This implies that the SP1 binding sites constitute an essential element of the *POR* proximal promoter. Indeed, SP1 binding sites as well as other noncore promoter elements are usually located in multiple copies within the proximal promoter region (~250 bp upstream of the transcription initiation site) of a ubiquitously expressed gene like *POR* (10). In this regard, several findings are noteworthy. First, the TATA box was apparently absent from the *POR* promoter region. This is compatible with the ubiquitous expression of *POR*, because the TATA box is usually identified in genes with a tissue-specific expression pattern (10). Second, the SP1 binding sites were highly conserved between the human and the rat. This finding, in conjunction with the previous data indicating absence of polymorphism for the three SP1 binding sites in 842 individuals (17), implies that the wild-type sequences of the SP1 binding sites are indispensable for the regulation of *POR* transcription. Third, the functional

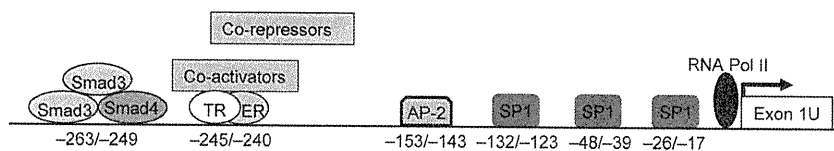


FIG. 5. Schematic representation indicating the binding sites for various factors in the proximal promoter region of *POR*. The diagram of the promoter upstream of -143 has been taken from Tee *et al.* (12). ER, Estrogen receptor; Pol II, polymerase II; TR, thyroid hormone receptor; AP-2, activator protein 2.

data using SL2 cells indicated a major role of SP1, rather than SP3, in the *POR* transcription. This is consistent with the notion that although both SP1 and SP3 can bind to the same cognate SP1 binding site, the DNA binding properties and regulatory functions are quite different between SP1 and SP3, depending on the promoter context and the cell type (18). Lastly, the SP1 binding sites were almost completely unmethylated. This argues for a transcriptionally active status of *POR*, because SP1 protein binding is known to be reduced when the CpG-rich region around the SP1 binding sites is methylated (19).

The proximal promoter region of *POR* has been studied previously (11, 12). Scott *et al.* (11) analyzed the 5' region of *POR* coding exons by means of comparative genomics and characterized human *POR* exon 1U and its flanking sequences. Subsequently, Tee *et al.* (12) examined a 361-bp region around the transcription start site of exon 1U ($-325/+36$) using adrenal NCI-H295A and liver Hep-G2 cells and found a major trophic effect of thyroid hormone on *POR* expression primarily via thyroid hormone receptor- β as well as modulatory effects of thyroid hormone receptor- α , estrogen receptor- α , Smad3, and Smad4 on *POR* expression. The binding sites for these factors reside in a $-263/-240$ region upstream of the SP1 binding sites (Fig. 5). Furthermore, Tee *et al.* (12) screened functional alterations of polymorphisms within the 325-bp region, suggesting that the common $-152C \rightarrow A$ polymorphism may play a certain role in the genetic variation of steroid biosynthesis and drug metabolism. In this regard, whereas the $-152C \rightarrow A$ polymorphism resides on the AP-2 (activator protein 2) binding site, the functional difference of the polymorphism is obviously independent of the recruit of AP-2 (12). Thus, the underlying factors for the reduced activity of the $-152A$ allele remain to be clarified.

Taken together, multiple regulatory elements have been identified in the proximal promoter region of *POR* (Fig. 5). Although the regulatory machinery has not yet been fully elucidated, we suggest that the presence of the SP1 binding sites has permitted the ubiquitous expression of *POR* and that the presence of other sites including thyroid hormone receptors is relevant to the variability in *POR* expression level among different tissues. In this regard, although the present study failed to identify the ef-

fects of the $-263/-240$ regulatory sequence identified by Tee *et al.* (12) (fragment D *vs.* fragment E in Fig. 2), this may be due to the difference in the cell type and/or in the promoter-luciferase construct used in the study by Tee *et al.* ($+36$) and in this study ($+99$). In addition, the hormonal effects on the *POR* transcription have not been ex-

amined in this study.

Finally, it would be useful to refer to clinical phenotypes of cases 1–3. In this context, we have previously compared clinical phenotype between Japanese PORD patients with homozygosity for the hypomorphic p.R457H mutation (group A) and those with compound heterozygosity for p.R457H and one apparently null mutation including nonsense and frameshift mutations (group B) and found that skeletal features are definitely more severe and adrenal dysfunction and 46,XY DSD are somewhat more severe in group B than in group A, whereas 46,XX DSD, maternal virilization during pregnancy, and anorectal and urinary anomalies are similarly identified in the two groups (5, 7). It is likely, therefore, that the residual *POR* activity reflected by the p.R457H dosage constitutes the underlying factor for clinical variability in some features but not in other features, probably due to the simplicity and complexity of *POR*-dependent metabolic pathways relevant to each phenotype. The clinical features of cases 1–3 are quite comparable to those of group B patients and, therefore, are consistent with transcription failure of one allele being a null mutation.

In summary, we identified microdeletions involving exon 1U and its upstream region in PORD patients, and revealed the critical function of the SP1 binding sites in the transcription of *POR*. Additional studies will permit to elucidate the regulatory machinery for *POR* expression.

Acknowledgments

We thank Dr. Timothy F. Osborne, University of California, Irvine, CA, and Dr. Guntram Suske, Philipps Universität, Marburg, Germany, for providing us with pPAC- β -galactosidase and pPAC-SP1/Sp3, respectively.

Address all correspondence and requests for reprints to: Dr. Maki Fukami, National Research Institute for Child Health and Development, Department of Endocrinology and Metabolism, 2-10-1 Ohkura, Setagaya, Tokyo 157-8535, Japan. E-mail: mfukami@nch.go.jp.

This work was supported by the Grant-in-Aid for Scientific Research on Innovative Areas (22132004) from the Ministry of Education, Culture, Sports, Science, and Technology (MEXT); by the Grant-in-Aid for Scientific Research (S) (22227002) from

the Japan Society for the Promotion of Science (JSPS); by the Grants for Research on Intractable Diseases (H22-098) and for Health Research on Children, Youth, and Families (H21-005) from the Ministry of Health, Labor and Welfare; by the Grant from Japan Foundation for Pediatric Research (10-001); and by the Grant of National Center for Child Health and Development (23A-1).

Disclosure Summary: The authors have nothing to declare.

References

- Flück CE, Tajima T, Pandey AV, Arlt W, Okuhara K, Verge CF, Jabs EW, Mendonça BB, Fujieda K, Miller WL 2004 Mutant P450 oxidoreductase causes disordered steroidogenesis with and without Antley-Bixler syndrome. *Nat Genet* 36:228–230
- Arlt W, Walker EA, Draper N, Ivison HE, Ride JP, Hammer F, Chalder SM, Borucka-Mankiewicz M, Hauffa BP, Malunowicz EM, Stewart PM, Shackleton CH 2004 Congenital adrenal hyperplasia caused by mutant P450 oxidoreductase and human androgen synthesis: analytical study. *Lancet* 363:2128–2135
- Miller WL 2004 P450 oxidoreductase deficiency: a new disorder of steroidogenesis with multiple clinical manifestations. *Trends Endocrinol Metab* 15:311–315
- Scott RR, Miller WL 2008 Genetic and clinical features of P450 oxidoreductase deficiency. *Horm Res* 69:266–275
- Fukami M, Nagai T, Mochizuki H, Muroya K, Yamada G, Takitani K, Ogata T 2010 Anorectal and urinary anomalies and aberrant retinoic acid metabolism in cytochrome P450 oxidoreductase deficiency. *Mol Genet Metab* 100:269–273
- Huang N, Pandey AV, Agrawal V, Reardon W, Lapunzina PD, Mowat D, Jabs EW, Van Vliet G, Sack J, Flück CE, Miller WL 2005 Diversity and function of mutations in P450 oxidoreductase in patients with Antley-Bixler syndrome and disordered steroidogenesis. *Am J Hum Genet* 76:729–749
- Fukami M, Nishimura G, Homma K, Nagai T, Hanaki K, Uematsu A, Ishii T, Numakura C, Sawada H, Nakacho M, Kowase T, Motomura K, Haruna H, Nakamura M, Ohishi A, Adachi M, Tajima T, Hasegawa Y, Hasegawa T, Horikawa R, Fujieda K, Ogata T 2009 Cytochrome P450 oxidoreductase deficiency: identification and characterization of biallelic mutations and genotype-phenotype correlations in 35 Japanese patients. *J Clin Endocrinol Metab* 94:1723–1731
- Shephard EA, Palmer CN, Segall HJ, Phillips IR 1992 Quantification of cytochrome P450 reductase gene expression in human tissues. *Arch Biochem Biophys* 294:168–172
- O'Leary KA, Kasper CB 2000 Molecular basis for cell-specific regulation of the NADPH-cytochrome P450 oxidoreductase gene. *Arch Biochem Biophys* 379:97–108
- Strachan T, Read AP 2004 Human gene expression. In: Strachan T, Read AP, eds. *Human molecular genetics*. 3rd ed. New York: Garland Science; 275–313
- Scott RR, Gomes LG, Huang N, Van Vliet G, Miller WL 2007 Apparent manifesting heterozygosity in P450 oxidoreductase deficiency and its effect on coexisting 21-hydroxylase deficiency. *J Clin Endocrinol Metab* 92:2318–2322
- Tee MK, Huang N, Damm I, Miller WL 2011 Transcriptional regulation of the human P450 oxidoreductase gene: hormonal regulation and influence of promoter polymorphisms. *Mol Endocrinol* 25:715–731
- Blondet A, Gout J, Durand P, Bégeot M, Naville D 2005 Expression of the human melanocortin-4 receptor gene is controlled by several members of the Sp transcription factor family. *J Mol Endocrinol* 34:317–329
- Di Nocera PP, Dawid IB 1983 Transient expression of genes introduced into cultured cells of *Drosophila*. *Proc Natl Acad Sci USA* 80:7095–7098
- Yazawa T, Mizutani T, Yamada K, Kawata H, Sekiguchi T, Yoshino M, Kajitani T, Shou Z, Miyamoto K 2003 Involvement of cyclic adenosine 5'-monophosphate response element-binding protein, steroidogenic factor 1, and Dax-1 in the regulation of gonadotropin-inducible ovarian transcription factor 1 gene expression by follicle-stimulating hormone in ovarian granulosa cells. *Endocrinology* 144:1920–1930
- Gu W, Zhang F, Lupski JR 2008 Mechanisms for human genomic rearrangements. *Pathogenetics* 1:4
- Huang N, Agrawal V, Giacomini KM, Miller WL 2008 Genetics of P450 oxidoreductase: Sequence variation in 842 individuals of four ethnicities and activities of 15 missense mutations. *Proc Natl Acad Sci USA* 105:1733–1738
- Li L, He S, Sun JM, Davie JR 2004 Gene regulation by Sp1 and Sp3. *Biochem Cell Biol* 82:460–471
- Zhu WG, Srinivasan K, Dai Z, Duan W, Druhan LJ, Ding H, Yee L, Villalona-Calero MA, Plass C, Otterson GA 2003 Methylation of adjacent CpG sites affects Sp1/Sp3 binding and activity in the p21(Cip1) promoter. *Mol Cell Biol* 23:4056–4065

Aromatase Excess Syndrome: Identification of Cryptic Duplications and Deletions Leading to Gain of Function of *CYP19A1* and Assessment of Phenotypic Determinants

Maki Fukami, Makio Shozu, Shun Soneda, Fumiko Kato, Akemi Inagaki, Hiroshi Takagi, Keiichi Hanaki, Susumu Kanzaki, Kenji Ohyama, Tomoaki Sano, Toshinori Nishigaki, Susumu Yokoya, Gerhard Binder, Reiko Horikawa, and Tsutomu Ogata

Department of Molecular Endocrinology (M.F., S.S., F.K., T.O.), National Research Institute for Child Health and Development, Tokyo 157-8535, Japan; Department of Reproductive Medicine (M.S.), Graduate School of Medicine, Chiba University, Chiba 206-8670, Japan; Department of Diabetes and Endocrinology (A.I., H.T.), Nagoya Second Red Cross Hospital Nagoya 466-8650, Japan; Department of Women's and Children's Family Nursing (K.H.) and Division of Pediatrics and Perinatology (S.K.), Tottori University, Yonago 683-8503, Japan; Department of Pediatrics (K.O., T.S.), Interdisciplinary Graduate School of Medicine and Engineering, University of Yamanashi, Chuo 408-3898, Japan; Department of Pediatrics (T.N.), Osaka Police Hospital, Osaka 543-0035, Japan; Department of Medical Subspecialties (S.Y., R.H.), National Medical Center for Children and Mothers, Tokyo 157-8535, Japan; and Pediatric Endocrinology Section (G.B.), University Children's Hospital, Tuebingen 72076, Germany

Context: Aromatase excess syndrome (AEXS) is a rare autosomal dominant disorder characterized by gynecomastia. Although cryptic inversions leading to abnormal fusions between *CYP19A1* encoding aromatase and its neighboring genes have been identified in a few patients, the molecular basis remains largely unknown.

Objective: The objective of the study was to examine the genetic causes and phenotypic determinants in AEXS.

Patients: Eighteen affected males from six families participated in the study.

Results: We identified three types of heterozygous genomic rearrangements, *i.e.* a 79,156-bp tandem duplication involving seven of 11 noncoding *CYP19A1* exons 1, a 211,631-bp deletion involving exons 2–43 of *DMXL2* and exons 5–10 of *GLDN*, and a 165,901-bp deletion involving exons 2–43 of *DMXL2*. The duplicated exon 1 functioned as transcription start sites, and the two types of deletions produced the same chimeric mRNA consisting of *DMXL2* exon 1 and *CYP19A1* coding exons. The *DMXL2* exon 1 harbored a translation start codon, and the *DMXL2/CYP19A1* chimeric mRNA was identified in only 2–5% of *CYP19A1*-positive transcripts. This was in contrast to the inversion-mediated chimeric mRNA that had no coding sequence on the fused exon 1 and accounted for greater than 80% of *CYP19A1*-positive transcripts. *CYP19A1* was expressed in a limited number of tissues, whereas its neighboring genes involved in the chimeric mRNA formation were expressed widely.

Conclusions: This study provides novel mechanisms leading to gain of function of *CYP19A1*. Furthermore, it appears that clinical severity of AEXS is primarily determined by the tissue expression pattern of relevant genes and by the structural property of promoter-associated exons of chimeric mRNA. (*J Clin Endocrinol Metab* 96: E1035–E1043, 2011)

Aromatase is a cytochrome P450 enzyme that plays a crucial role in the estrogen biosynthesis (1). It catalyzes the conversion of Δ^4 -androstendione into estrone and that of testosterone (T) into estradiol (E_2) in the placenta and ovary as well as in other tissues such as the fat, skin, bone, and brain (1). It is encoded by *CYP19A1* consisting of at least 11 noncoding exons 1 and nine coding exons 2–10 (Supplemental Fig. 1, published on The Endocrine Society's Journals Online web site at <http://jcem.endojournals.org>) (2, 3). Each exon 1 is accompanied by a tissue-specific promoter and is spliced alternatively onto a common splice acceptor site at exon 2, although some transcripts are known to contain two of the exons 1, probably due to a splice error (2, 4). Of the 11 exons 1, exon I.4 appears to play a critical role in the regulation of estrogen biosynthesis in males because this exon contains a major promoter for extragonadal tissues including the skin and fat (2).

Excessive *CYP19A1* expression causes a rare autosomal dominant disorder known as aromatase excess syndrome (AEXS) (5–8). AEXS is characterized by pre- or peripubertal onset gynecomastia, advanced bone age from childhood to the pubertal period, and short adult height in affected males (5–8). Affected females may show several clinical features such as macromastia, precocious puberty, irregular menses, and short adult height (6–8). In this regard, previous studies have identified four heterozygous cryptic inversions around *CYP19A1* in patients with AEXS (5, 8). Each inversion results in the formation of a chimeric gene consisting of a noncoding exon(s) of a neighboring gene (*CGNL1*, *MAPK6*, *TMOD3*, or *TLN2*) and coding exons of *CYP19A1*. Because this condition is predicted to cause aberrant *CYP19A1* expression in tissues in which each neighboring gene is expressed, such inversions have been regarded to be responsible for AEXS (5, 8).

However, such inversions have been revealed only in a few patients with AEXS, and, despite extensive studies, no other underlying genetic mechanisms have been identified to date (6, 8–10). Here we report novel genomic rearrangements in AEXS and discuss primary phenotypic determining factors in AEXS.

Patients and Methods

Patients

This study was approved by the Institutional Review Board Committee at the National Center for Child Health and Development and was performed after obtaining informed consent. We examined 18 male patients aged 8–69 yr (cases 1–18) from six unrelated families A–F (Fig. 1A). The probands were ascertained by bilateral gynecomastia (Fig. 1B) and the remaining 12 males by familial studies. Ten other males allegedly had gynecomastia. There were four obligatory carrier females.

Phenotypic assessment showed pre- or peripubertal onset gynecomastia in all cases, small testes and fairly preserved masculinization in most cases, obvious or relative tall stature in childhood and grossly normal or relative short stature in adulthood, and age-appropriate or mildly advanced bone ages (Table 1) (for detailed actual data, see Supplemental Table 1). Such clinical features, especially gynecomastia, tended to be milder in cases 1–4 from families A and B than in the remaining cases from families C–F. Fertility or spermatogenesis was preserved in all adult cases (≥ 20 yr). In addition, the obligatory carrier females from families B and D had apparently normal phenotype, and such females from families E and F exhibited early menarche (9.0 yr) and short adult stature (-2.8 SD), respectively.

Blood endocrine studies revealed that LH values were grossly normal at the baseline and variably responded to GnRH stimulation, whereas FSH values were low at the baseline and responded poorly to GnRH stimulation, even after preceding GnRH priming (Table 1) (for detailed actual data, see Supplemental Table 1) (see also Fig. 1C for the cases aged ≥ 15 yr). Δ^4 -Androstendione, T, and dihydrotestosterone values were low or normal. A human chorionic gonadotropin (hCG) test indicated relatively low but normal T responses in five young cases. In most cases, estrone values were elevated, E_2 values were normal or elevated, and E_2/T ratios were elevated. These endocrine data were grossly similar among cases 1–18.

Aromatase inhibitor (anastrozole, 1 mg/d) was effective in all the four cases treated (Supplemental Table 1) (see also Fig. 1C for cases aged ≥ 15 yr). Gynecomastia was mitigated within 6 months of treatment, and endocrine data were ameliorated within 1 month of treatment.

Primers

Primers used in this study are shown in Supplemental Table 2.

CYP19A1 mRNA levels and aromatase activities

We analyzed relative mRNA levels of *CYP19A1* and catalytic activities of aromatase in skin fibroblasts (SF) and lymphoblastoid cell lines (LCL). mRNA were extracted by a standard method and were subjected to RT-PCR using a high capacity RNA-to-cDNA kit (Life Technologies, Carlsbad, CA). A relative amount of *CYP19A1* mRNA against *B2M* was determined by the real-time PCR method using the Taqman gene expression assay on ABI PRISM 7500fast (Life Technologies) (assay no. Hs00903411_m1 for *CYP19A1* and Hs99999907_m1 for *B2M*). PCR was performed in triplicate. Aromatase activity was determined by a tritium incorporation assay (11). In brief, the samples were incubated with androstenedione-2- 3 H for 2 h, and 3 H H_2O in the supernatant of the culture media was measured with a scintillation counter LSC-5100 (Aloka, Tokyo, Japan).

Sequence analysis of CYP19A1

Leukocyte or SF genomic DNA samples from the six probands and additional four male patients (Fig. 1A) were PCR amplified for the coding exons 2–10 and their flanking splice sites of *CYP19A1*. Subsequently the PCR products were subjected to direct sequencing from both directions on CEQ 8000 autosequencer (Beckman Coulter, Fullerton, CA).

Genome structure analysis

Oligonucleotide array-based comparative genomic hybridization (CGH) analyses were carried out using a custom-built

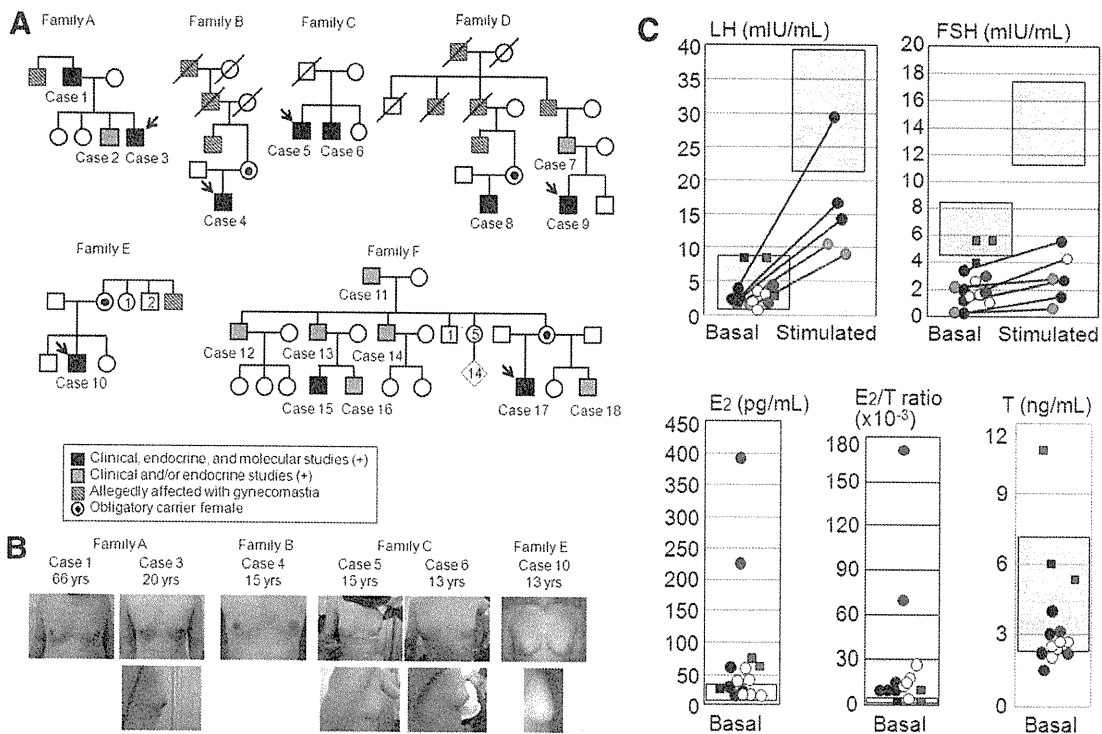


FIG. 1. Summary of clinical data. A, Pedigrees of six families with patients exhibiting AEXS-compatible phenotype. Families A–E are of Japanese origin, and family F is of German origin. Cases from families A–D were hitherto unreported, whereas those from families E and F have previously been described as having AEXS phenotypes (6, 8). B, Gynecomastia of six cases. C, Endocrine data in cases 15 yr of age or older. The black, white, and red colors represent the data in cases of the duplication, the deletion, and the inversion types, respectively; the blue color indicates the data of GnRH test after GnRH priming in two cases of the duplication type. The data at the time of diagnosis are denoted by circles, and those on aromatase inhibitor (anastrozole) treatment (1 mg/d in the duplication and the deletion types and 2–4 mg/d in the inversion types) are depicted by squares. The light purple areas represent the normal reference ranges.

oligo-microarray containing 90,000 probes for the 15q11.2-q26.3 region and approximately 10,000 reference probes for other chromosomal region ($2 \times 105K$ format, design identification 026533) (Agilent Technologies, Palo Alto, CA). The procedure was as described in the manufacturer’s instructions. Fluorescence *in situ* hybridization (FISH) analysis was performed for lymphocyte or SF metaphase spreads, using long PCR products (FISH probes 1 and 2) for rearranged regions and CEP 15 probe for *D15Z4* used as an internal control (Abbott, Abbott Park, IL). The FISH probes 1 and 2 were labeled with digoxigenin and detected by rhodamine antidigoxigenin, and the CEP 15 probe was detected according to the manufacturer’s protocol.

Characterization of the duplications and deletions

The duplication junctions were determined by direct sequencing for standard PCR products obtained with a variety of combinations of primers hybridizing to different positions within the *CYP19A1* exons 1 region. The deletion junctions were identified by direct sequencing of the long PCR products obtained with primer pairs flanking the deletions. The sizes of duplications and the deletions were determined by comparing obtained sequences with NT_010194 sequences at the National Center for Biotechnology Information Database (<http://www.ncbi.nlm.nih.gov/>; Bethesda, MD). The presence or absence of repeat sequences around the breakpoints was examined with Repeatmasker (<http://www.repeatmasker.org>).

For mRNA analysis, we performed 5’-rapid amplification of cDNA ends (RACE) using a SMARTER RACE cDNA ampli-

cation kit (Takara Bio, Ohtsu, Japan). For both duplications and deletions, first PCR was carried out using the forward primer mix provided in the kit (Universal primer A mix) and an antisense reverse primer specific to *CYP19A1* exon 3 (RACE Rev). Second PCR was carried out for diluted products of the first PCR, using the nested forward primer of the kit (Nested universal primer A) and a reverse primer for *CYP19A1* exon 2 (Nested Rev). For duplications, furthermore, second PCR was also performed using various combinations of primers hybridizing to each *CYP19A1* exon 1. Subsequently PCR products were subcloned into TOPO cloning vector (Life Technologies) and subjected to direct sequencing. Then, the obtained sequences were examined with BLAST Search (National Center for Biotechnology Information). The presence or absence of promoter-compatible sequences was analyzed with the University of California, Santa Cruz, genome browser (<http://genome.ucsc.edu/>).

Relative mRNA levels of *CYP19A1* and its neighboring genes

We investigated relative mRNA levels of *CYP19A1* and *DMXL2* as well as those of *CGNL1*, *MAPK6*, *TMOD3*, and *TLN2* involved in the previously reported cryptic inversions (5, 8) in various human tissues. In this experiment, cDNA of SF and LCL were obtained from control males, and the remaining human cDNA samples were purchased from Life Technologies or Takara Bio. Relative quantification of mRNA against *TBP* was carried out using Taqman gene expression assay kit

TABLE 1. Summary of clinical studies in male patients with aromatase excess syndrome^a

	Present study						Previous studies			
	Family A	Family B	Family C	Family D	Family E	Family F	Family 1	Family 2	Sporadic	
Cases	Cases 1–3	Case 4	Cases 5–6	Cases 7–9	Case 10	Cases 11–18	Two cases ^b	Proband ^c	Patient 1	Patient 2
Mutation type	Duplication	Duplication	Deletion	Deletion	Deletion	Deletion	Inversion	Inversion	Inversion	Inversion
Phenotypic findings										
Gynecomastia	Yes (mild)	Yes (mild)	Yes (moderate)	Yes (moderate)	Yes (moderate)	Yes (moderate)	Yes (severe)	Yes (severe)	Yes (severe)	Yes (severe)
Pubertal defect	Yes (mild)	Yes (mild)	Yes (mild)	No	No	Yes (mild)	N.D.	Yes (mild)	No	N.D.
Short adult height	No	No	N.D.	No	N.D.	No	Yes	N.D.	Yes	N.D.
Spermatogenesis	Preserved	N.D.	N.D.	Preserved	N.D.	Preserved	Preserved	N.D.	N.D.	N.D.
Endocrine findings										
LH (basal)	Normal	Normal	Normal	Normal/low	Normal	Normal/low	Normal	Normal/low	Normal	N.E.
LH (GnRH stimulated) ^d	Low	Normal	High	Normal	Normal	Normal	N.E.	Low	N.E.	N.E.
FSH (basal)	Low	Low	Low	Low	Low	Normal/low	Normal/low	Low	Low	N.E.
FSH (GnRH stimulated) ^d	Low	Low	Low	Low	Low	Low	N.E.	Low	N.E.	N.E.
T (basal)	Normal/low	Normal	Normal/low	Normal/low	Normal	Normal/low	Normal	Normal/low	Low	N.E.
T (hCG stimulated) ^e	N.E.	N.E.	Normal	Normal	Normal	Normal	N.E.	Normal	N.E.	N.E.
E ₁ (basal)	High	High	N.E.	High	High	High	High	High	High	N.E.
E ₂ (basal)	Normal	High	High	Normal	High	Normal/high	High	High	High	N.E.
E ₂ to T ratio	High	High	High	High	High	High	High	High	High	N.E.

E₁, Estrone; N.D., not determined; N.E., not examined.

^a Detailed actual data are shown in Supplemental Table 1.

^b A father-son pair.

^c The sister has macromastia, large uterus, and irregular menses; the parental phenotype has not been described.

^d GnRH 100 $\mu\text{g}/\text{m}^2$ (maximum 100 μg) bolus iv; blood sampling at 0, 30, 60, 90, and 120 min.

^e hCG 3000 IU/m² (maximum 5000 IU) im for 3 consecutive days; blood sampling on d 1 and 4.

(assay no. Hs00903411_m1 for *CYP19A1*; Hs00324048_m1 for *DMXL2*; Hs00262671_m1 for *CGNL1*; Hs00833126_g1 for *MAPK6*; Hs00205710_m1 for *TMOD3*; Hs00322257_m1 for *TLN2*; and Hs99999910_m1 for *TBP*). The experiments were carried out three times.

Results

CYP19A1 mRNA levels and aromatase activities

Although relative mRNA levels of *CYP19A1* and catalytic activities of aromatase were grossly similar between LCL of case 3 (family A), case 4 (family B), and case 5 (family C) and those of control subjects, they were significantly higher in SF of case 3 (family A), case 4 (family B), case 9 (family D), and case 10 (family E) than in those of control subjects (Fig. 2).

Sequence analysis of *CYP19A1*

Direct sequencing showed no mutation in *CYP19A1* coding exons 2–10 of the 10 cases examined.

Genome structure analysis

CGH analysis revealed heterozygous cryptic duplications involving most of the *CYP19A1* exons 1 region in cases from families A and B, heterozygous cryptic deletions involving most of *DMXL2* and part of *GLDN* in cases from family C, and heterozygous cryptic deletions involving most of *DMXL2* in cases from families D–F (Fig.

3A). FISH analysis supported the duplications and confirmed the deletions.

Characterization of the cryptic duplications

Aberrant PCR products were obtained with the P2 primer (which amplifies a segment between exon I.1 and exon IIa with the P1 primer) and the P3 primer (which amplifies a segment between exon I.2 and exon I.6 with the P4 primer), and sequencing of the PCR products showed the same tandem duplication involving seven of the 11 exons 1 of *CYP19A1* in cases from families A and B (Fig. 3B). The duplicated region was 79,156-bp long, and the

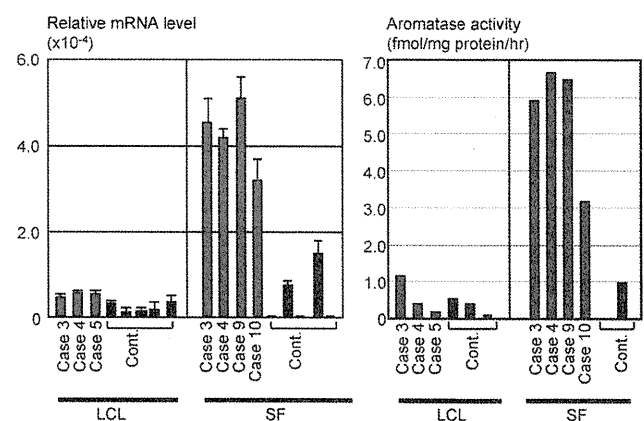


FIG. 2. Relative *CYP19A1* mRNA levels against *B2M* and catalytic activities of aromatase.

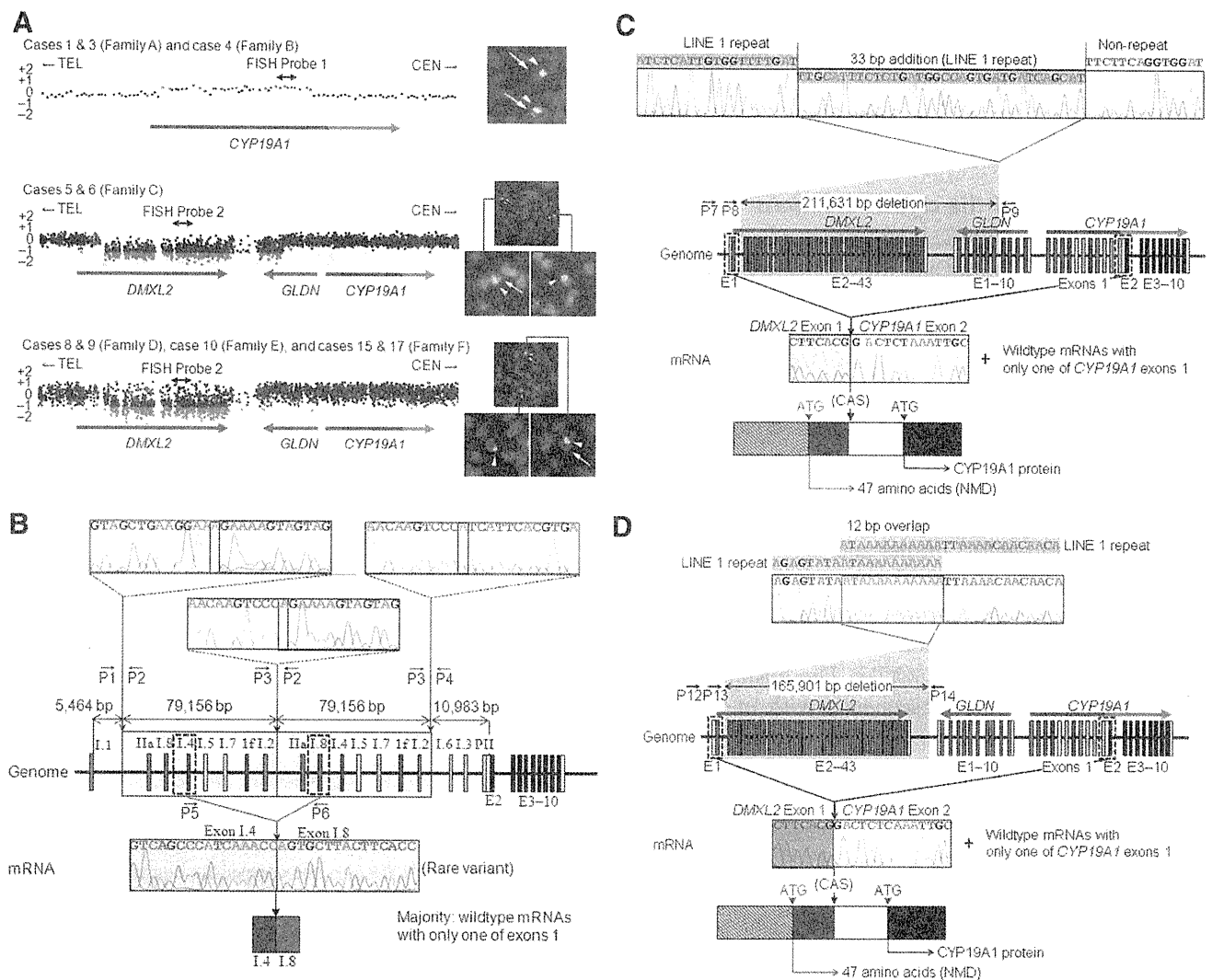


FIG. 3. Summary of molecular studies. For *CYP19A1*, the dark and light blue lines represent the genomic regions for noncoding exons 1 and coding exons 2–10, respectively. **A**, Oligoarray CGH and FISH analyses. In CGH analysis, the black, red, and green dots denote signals indicative of the normal, the increased (>+0.5), and the decreased (<-1.0) copy numbers, respectively. In FISH analysis, two red signals with an apparently different density are identified in cases from families A and B by FISH probe 1, whereas only a single red signal is found in cases from families C–F by FISH probe 2. The green signals are derived from the internal control probe. **B**, Schematic representation of the tandem duplication shared in common by cases 1 and 3 from family A and case 4 from family B. Genome, The junction sequence of the tandem duplication (yellow boxes) is shown, together with the original normal sequences at the 5'- and the 3'-ends of the duplicated region. The sequences highlighted with light green and light orange are identical, and 1 bp (A) is shared at the junction point (highlighted with light yellow). mRNA, The sequence of a rare clone is shown. The 3'-end of exon I.4 is connected with the 5'-end of exon I.8. **C**, Schematic representation of the deletion in sibling cases 5 and 6 from family C. Genome, The junction sequence of the deletion (a gray area) is shown. The fusion has occurred between a LINE 1 repeat sequence (highlighted with blue) at intron 1 of *DMXL2* and a nonrepeat sequence at intron 4 of *GLDN* and is accompanied by an addition of a 33-bp segment with a LINE 1 repeat sequence. mRNA, The sequence of a rare chimeric gene transcript is shown. *DMXL2* exon 1 consisting of a noncoding region (a red striped box) and a coding region (a red box) is spliced onto the common acceptor site (CAS) of *CYP19A1* exon 2 comprising an untranslated region (a white box) and a coding region (a black box). Thus, this transcript has two translation initiation codons (ATG), although the mRNA destined to produce a 47-amino acid protein from the ATG on *DMXL2* exon 1 is predicted to undergo NMD. **D**, Schematic representation of the deletion shared in common by cases 8 and 9 from family D, case 10 from family E, and cases 15 and 17 from family F. Genome, The junction sequence of the deletion (a gray area) is shown. The fusion has occurred between a LINE 1 repeat sequence (highlighted with blue) at intron 1 of *DMXL2* and that at a downstream region of *DMXL2*, with an overlap of a 12-bp segment. mRNA, The sequence of a chimeric gene transcript is delineated. The mRNA structure is the same as that described in the legend for Fig. 3C.

fusion occurred between nonrepeat elements with an overlap of one nucleotide.

All the 5'-RACE products (>500 clones) obtained from LCL and SF of case 3 (family A) and case 4 (family B) were found to be associated with a single exon 1, as observed in

control materials. However, PCR amplifications for the 5'-RACE products with a variety of combinations of primers hybridizing to each exon 1 and subsequent sequencing of the PCR products revealed the presence of a chimeric clone consisting of exon I.4 at the 5' side and exon I.8 at